

Anatomical basis of sex differences in human post-myocardial infarction ECG phenotypes identified by novel automated torso-cardiac 3D reconstruction

Hannah J. Smith¹, Blanca Rodriguez¹, Yuling Sang², Marcel Beetz², Robin P. Choudhury³, Vicente Grau², and Abhirup Banerjee^{2,3}

¹ Computational Cardiovascular Science Group, Department of Computer Science, University of Oxford, Oxford OX1 3QD, United Kingdom

² Institute of Biomedical Engineering, Department of Engineering Science, University of Oxford, Oxford OX3 7DQ, United Kingdom

³ Division of Cardiovascular Medicine, Radcliffe Department of Medicine, University of Oxford, Oxford OX3 9DU, United Kingdom

*Address for correspondence.

Abhirup Banerjee, Institute of Biomedical Engineering, Department of Engineering Science, University of Oxford, Oxford OX3 7DQ, United Kingdom, abhirup.banerjee@eng.ox.ac.uk

Acknowledgements. This research has been conducted using the UK Biobank Resource under Application Number '40161'. HJS is supported by a Wellcome Trust Studentship. AB is a Royal Society University Research Fellow and is supported by the Royal Society Grant No. URF\R1\221314. The works of AB, RPC, and VG are supported by the British Heart Foundation (BHF) Project under Grant PG/20/21/35082. This work was funded by a Wellcome Trust Fellowship in Basic Biomedical Sciences to BR (214290/Z/18/Z) and the CompBioMed 2 Centre of Excellence in Computational Biomedicine (European Commission Horizon 2020 research and innovation programme, grant agreements No. 823712) to BR and VG. The authors would like to thank Dr Ernesto Zacur for providing valuable suggestions on the 3D anatomical mesh reconstruction.

Competing interests. The authors declare no competing interests.

Author contributions. HJS, BR, VG, and AB conceptualised the study and designed the research. BR, VG, RPC, and AB supervised the research. HJS and AB acquired and curated the dataset. AB and HJS developed the reconstruction pipeline. HJS, AB, YS, and MB pre-processed and cleaned the data. HJS and AB conducted the study and analysed the data and the results. HJS, AB, BR, and VG prepared the original draft and reviewed and edited the manuscript. All authors discussed the results, provided comments regarding the manuscript, and agreed on the final draft.

Data availability. The UK Biobank data is publicly available and can be accessed by application upon approval here: <https://www.ukbiobank.ac.uk/enable-your-research/register>.

Code availability. The codes used to create the models and perform analysis were implemented on multiple programming platforms and can be accessed by contacting the corresponding author upon a reasonable request.

Abstract

The electrocardiogram (ECG) is routinely used in cardiology, though its interpretation is confounded by anatomical variability. A novel, automated computational pipeline enables quantification of torso-ventricular anatomy metrics from magnetic resonance imaging, and comparison to ECG characteristics. Sex and myocardial infarction differences are investigated based on 1051 healthy and 425 post-MI subjects from UK Biobank. Smaller ventricles in females explain ~50% of shorter QRS durations than in males, and contribute to lower STJ amplitudes in females (also due to more superior and posterior position). In females, torso-ventricular anatomy, particularly from larger BMI, is a stronger modulator of T wave amplitude reductions and left-deviated R axis angles in post-MI than in males. Thus, female MI phenotype is less reflective of pathology, and baseline STJ amplitudes and QRS durations are further from clinical thresholds. Therefore, quantification of anatomical sex-differences and impact on ECG in health and disease is critical to avoid clinical sex-bias.

The electrocardiogram (ECG) is a vital tool for routine clinical assessment of cardiac electrical abnormalities. However, the relative position and orientation of the heart with respect to the electrode locations can affect ECG complex morphology. Computational and experimental studies have demonstrated that torso-ventricular orientation can substantially affect the ECG, potentially confounding disease diagnosis, and that ECG variability due to anatomy exceeds that of electrophysiology in healthy subjects [1-5].

van Oosterom et al. [6] compared magnetic resonance images (MRIs) and ECGs of 15 healthy patients and found that the crucial factors for determining ECG amplitudes are the size of the ventricles and the distance between the myocardium and ECG electrodes. Dispersion in ECG biomarkers between leads further demonstrates that the recording of the same electrical event is heavily influenced by the location of each electrode relative to the myocardium [7]. However, these investigations rely on manual torso segmentation from a very limited number of subjects. The investigation of population-wide trends requires automated torso reconstruction from clinically standard cardiac magnetic resonance (CMR) imaging to facilitate high-throughput analysis of the ECG-anatomy relationship.

Sex differences in ECG biomarkers are age-dependent – significantly appearing during adolescence, peaking in early to mid-adulthood, and largely declining with older age [8]. Female ECGs typically exhibit shorter QRS durations and lower ST junction (STJ) and T wave amplitudes, but longer QT intervals, than male [8]. The origin of these differences is multifactorial, with both electrophysiological and structural factors contributing. Testosterone increases repolarising potassium currents and decreases L-type calcium currents, both acting to speed up repolarisation [9]. Additionally, left ventricular mass is smaller in females than males [10], a factor known to affect QRS duration and STJ and T wave amplitudes [11, 12]. Decreases in torso volume are known to increase QRS and T wave amplitudes [1, 2], making the smaller female torso a potential contributor to ECG sex differences, but the impact on STJ amplitude and the relative size of the effect on all biomarkers is not known. Sex differences in cardiac position have been noted, particularly in the superior-inferior axis [13]. However, differences in the post-MI population and the quantification of the effect of these anatomical differences on key ECG biomarkers, in comparison with the effects of electrophysiological sex differences, is largely unknown.

Interpretation of the ECG is particularly important for the clinical assessment of acute myocardial infarction (MI) patients. Acutely, ischemic ECG changes are a fundamental consideration in diagnosis and categorisation of MI events [14]. Changes to the ST segment are particularly important in this context, with ST-elevation MI (STEMI), mandating immediate reperfusion therapy [15, 16]. There is a higher incidence of missed diagnosis of acute MI in females, and hospital care can be less aggressive [17-21]. This is a potential contributor to the higher female mortality following MI [22, 23], alongside factors such as differing demographic risk characteristics and comorbidities [21, 24, 25]. Therefore, it is critical to understand how anatomical sex differences may contribute to the baseline STJ amplitude in order to improve interpretation of any increases during an acute MI event.

Following MI, risk stratification tools are used to identify patients susceptible to sudden cardiac death (SCD), primarily from ventricular arrhythmias [26]. However, current risk stratification guidelines that primarily focus on the left ventricular ejection fraction (LVEF) fail to identify the majority of SCD cases, prompting calls for supplemental ECG biomarkers to be used [27]. These include measures of slowed conduction, such as QRS duration, which can increase following MI [28, 29] and of increased repolarisation heterogeneity, which are affected by the duration, amplitude, and axis angles of the QRS and T waves [30, 31]. However, as variation of anatomical factors has been shown to exceed thresholds for diagnosing pathology [2, 3], without correction for anatomy,

their use is fundamentally problematic. The intersectional relationship between the anatomy and demographic features indicates that the accuracy of ECG interpretation will be skewed by characteristics such as sex and body mass index (BMI) if these factors are not considered [9, 32, 33]. Therefore, it is important to investigate the effect of sex and BMI differences on parameters considered for integration into risk stratification tools following MI such as QRS duration, T wave amplitude, and R and T axis angles. BMI is a critical parameter to consider, as patients with an MI history are more likely to have higher BMI, which may change the cardiac orientation [32, 34-36]. However, any sex differences in these anatomical changes, or in the sensitivity of ECG biomarkers to them, is yet to be studied. Female electrophysiological remodelling post-infarction has been reported to be less detrimental than male, partially due to the protective effects of estrogen [37]. This suggests that the anatomical differences from increased BMI may be proportionally more significant than in males where the electrophysiological differences may be greater.

Accordingly, our current work aims to (1) develop and validate an automated image processing pipeline to reconstruct 3D torso models using clinically standard CMR images in the UK Biobank study [38], (2) quantify differences in torso-ventricular anatomy and ECG biomarkers, and (3) identify the key anatomical determinants of ECG biomarkers for healthy and chronic-stage post-MI subjects of both sexes. We hypothesise that whereas the smaller female heart and torso could explain baseline sex differences in some ECG parameters, sex variation in healthy versus post-MI subjects will primarily be related to the effects of increased BMI on torso volume and cardiac orientation. Anatomical effects may be proportionally more significant in females than males due to their predicted smaller electrophysiological changes. In order to explore this, we have developed a novel end-to-end automated image processing pipeline to first segment and extract the torso boundaries from clinically standard CMR images and then optimally reconstruct the personalised 3D torso model from the sparse point cloud. We have analysed this pipeline over 1051 healthy and 425 post-MI subjects to investigate sex differences in the relationship between torso-ventricular anatomy and key ECG biomarkers in healthy and post-MI patients. These insights will lay the groundwork for a process to correct for the effect of differing torso-ventricular anatomy on the ECG, enabling personalised, automated ECG interpretation.

Results

Reconstructed surfaces matched input contours to within 2.19mm:

Figure 1 shows the pipeline used to create the 3D torso reconstructions. Figure 2A demonstrates that the three-stage segmentation, automated post-processing, and refinement procedure improved torso contour extraction, compared with a single-stage contouring network, across all image views. This increased the median Dice coefficient over the independent test subjects from 0.76 to 0.95. The median surface-to-contour distance, showing the quality of the reconstructed torso surface, as shown in Figure 2B, for the test subjects was 2.19mm (inter-quartile range - IQR: 1.98-2.37mm). The median surface-to-surface distance between torso meshes reconstructed using the manually annotated contours and the machine learning pipeline for the 30 test subjects was 0.82mm (IQR: 0.69-1.10mm). Figure 2C shows the reconstructed surfaces for the test subjects with the smallest and largest median reconstruction errors. They are coloured by the distance from the surface reconstructed using the automated pipeline to that using the manually annotated contours, showing the error propagation from the 2D image segmentation to 3D reconstruction. Both reconstructed surfaces are smooth and anatomically realistic, and across most of the torso errors are within the millimetre range. On the worst performing subject there appears to be a rotational error affecting the performance in the lower right-hand quadrant of the torso, causing errors on the centimetre

range. The distance between each electrode reconstructed using the manually annotated contours and the machine learning pipeline had a median of 1.28mm (IQR: 0.90-1.97mm).

Approximately 50% of female versus male QRS differences is explained by small cavity volumes:

Figures 3A and 3B show that for both healthy and post-MI subjects, QRS duration was shorter in females versus males in all leads; for example, in healthy subjects the mean shortening from males to females across leads was 6.0 ± 1.5 ms. Figures 3C and 3D show the contribution of each anatomical factor and the remaining effect of electrophysiology, to the difference between female and male QRS duration. Healthy and post-MI subjects are plotted separately. In healthy subjects, this shows that cavity volume, enclosed by the endocardial surfaces of both ventricles, contributed between 0.7 ± 0.8 ms and 4.5 ± 0.8 ms with a mean across all leads of 3.4 ± 1.3 ms, therefore contributing approximately half of the 6.0 ± 1.5 ms mean total sex difference. Similarly for post-MI subjects, cavity volume contributed a mean of 4.5 ± 1.4 ms of a total sex difference of 8.3 ± 2.5 ms. The effect of electrophysiology consistently contributed between 1.0 ± 1.0 ms and 2.3 ± 1.2 ms to the sex difference in the precordial leads for healthy subjects; but in post-MI subjects, the electrophysiological contribution was considerably more variable, increasing markedly from 0.2 ± 2.8 ms in V1 to 6.3 ± 3.0 ms in V6. The total sex difference in QRS duration was largest in lead aVL – healthy females had a QRS duration 8.7 ± 1.0 ms shorter than males and correspondingly post-MI females had 11.5 ± 2.3 ms shorter.

In post-MI patients, torso volume was larger by 3.7 ± 0.9 dm³ ($10.2 \pm 3.3\%$) and 3.5 ± 0.5 dm³ ($8.2 \pm 1.9\%$) in females and males respectively; for post-MI subjects, the heart was positioned more posteriorly in females by 3.1 ± 0.9 mm and oriented with its long axis more horizontally by $6.0 \pm 1.2^\circ$ and $4.3 \pm 0.5^\circ$ in females and males respectively. Distributions of all anatomical parameters are shown in Supplemental Figure 2. All of these changes were related to the increased BMI of post-MI subjects, as shown in Supplemental Figure 2K. Figures 3E and 3F demonstrate that the QRS prolongation in MI compared with healthy populations was again less substantial in females than males with mean percentage reduction in QRS duration, across all leads, of $3.4 \pm 2.3\%$ and $5.8 \pm 1.5\%$ respectively. Figures 3G and 3H show the contribution of each anatomical factor and the remaining effect of electrophysiology, to the difference between healthy and post-MI subjects' QRS durations. Females and males are shown separately. Comparing Figures 3G and 3H demonstrates that the reduced amount of QRS duration prolongation following MI in females over males was associated with smaller electrophysiological contributions. There was also an increased amount of compensating shortening in QRS duration (shown as negative contributions) from anatomical factors, primarily torso volume. For both females and males, the more horizontal cardiac long axis in post-MI compared with healthy subjects was associated with a substantial proportion of their QRS prolongation for all precordial, and most limb, leads.

STJ amplitude is lower in females than males in all precordial leads for healthy and post-MI subjects, explained by a smaller left ventricular (LV) mass and more superior and posterior position:

Figure 4A and Supplemental Figure 5A show that for both healthy and post-MI subjects, STJ amplitude, measured at the end of the QRS complex, is significantly lower in the precordial leads in females versus males, particularly in the septal and anterior leads. Figure 4B and Supplemental Figure 5B show anatomical and electrophysiological contributions to this STJ amplitude sex difference. They demonstrate that this can be partly explained by females' decreased LV mass (by $29.3 \pm 5.4\%$ and $27.1 \pm 5.7\%$ in healthy and post-MI subjects respectively), 9.6 ± 0.9 mm more superior position for healthy subjects, and 4.3 ± 1.0 mm more posterior position for post-MI subjects. While

females' smaller LV mass generally added to the electrophysiological sex difference, their smaller torso volume had a negative contribution, as a smaller torso volume was generally associated with a higher STJ amplitude. Baseline STJ amplitude in lead V4 was 0.028 ± 0.003 mV lower in healthy females than healthy males. As BMI positively correlates with torso volume, this meant that for healthy females with $\text{BMI} > 25 \text{ kgm}^{-2}$ STJ amplitude was 0.047 ± 0.004 mV lower than for healthy males with $\text{BMI} < 25 \text{ kgm}^{-2}$.

T wave amplitude (TWA) following MI is more associated with a more posterior cardiac position and more horizontal orientation in females than males:

Figures 4C and D show that in females, TWA was only substantially reduced following MI in precordial leads V4-6, alongside most limb leads, whereas in males this occurred in all leads. Figures 4E and 4F show anatomical and electrophysiological contributions to the TWA reduction following MI. They demonstrate that for both females and males the reduced verticality and larger torso volume of post-MI subjects compared with healthy controls contribute to their reduced TWA; but in females the more posterior position also plays a role. The more posterior post-MI cardiac position and more horizontal orientation play an important role in TWA in females compared to males. The remaining difference after anatomical effects were considered, estimating the electrophysiological component, for males was consistently associated with reduced TWA in the precordial leads, primarily the anterior leads (V3-V4). However, in females this was actually associated with increased TWA in the septal leads (V1-V2), with significant reductions only in the lateral leads (V5-V6). These increases are however masked by the negative contribution of anatomical factors, such as posterior position and torso volume, leading to little difference in the TWA for the septal and anterior leads in females.

R axis deviations following MI are associated with cardiac orientation in females, but electrophysiology in males:

Whereas the previous ECG parameters can be assessed in individual leads, ECG-derived axis angles are a composite metric. They are positively correlated with amplitudes in leads exploring the superior-inferior direction, such as lead aVF, and negatively correlated with those exploring the lateral-medial direction, such as lead I [39]. Figures 5A and 5B show anatomical and electrophysiological contributions to R and T axis deviation following MI separately for females and males. They demonstrate that for females, the $5.3 \pm 4.0^\circ$ left deviation in the R axis is mainly associated with a more horizontal cardiac long axis, with electrophysiological factors playing very little role. However, for males the electrophysiological contribution dominates their $12.0 \pm 2.8^\circ$ left deviated R axis. This is partly explained by female R axes being more sensitive to changes in verticality, as shown by its higher regression coefficient in Figure 5C. The female T axis was more right deviated than that for males, largely associated with electrophysiology.

Figure 5E reveals torso volume significantly affected R axis for both sexes in healthy, but not post-MI subjects. For example, in healthy females, every 10 dm^3 increase in torso volume was associated with a decrease in R axis of $7.2 \pm 3.0^\circ$. This was related to increased distance to the LL electrode (inversely related to the R axis) without as substantial an increase in distance to the LA electrode (positively related to the R axis). For healthy females, every 10 dm^3 increase in torso volume was associated with an increased distance to the heart centre of $19.4 \pm 0.7 \text{ mm}$ and $5.9 \pm 0.6 \text{ mm}$ for the LL and LA electrodes, respectively. However, in post-MI females, the gap between these differences was smaller, with corresponding increased distances of $16.6 \pm 1.8 \text{ mm}$ and $8.3 \pm 1.7 \text{ mm}$. Similar trends for healthy males mean that the difference in R axis between subjects with a $\text{BMI} < 25 \text{ kgm}^{-2}$ and $\text{BMI} > 25 \text{ kgm}^{-2}$ is $19.1 \pm 3.3^\circ$, whereas for post-MI males it is only $5.5 \pm 5.2^\circ$.

Discussion

This study provides a comprehensive evaluation of the interplay between anatomy and key ECG biomarkers, and the way in which the intersectional effect of previous myocardial infarction and sex mediates this relationship. The development and validation of a novel image processing pipeline for automated 3D torso reconstruction enables high-throughput investigations into the effects of anatomical variability on the study of a wide range of cardiac diseases. The adaptation of the pipeline to standard clinical cardiac imaging allows for the exploitation of extensive databases, such as the UK Biobank, and sets the groundwork for clinical tools to personalise ECG interpretation by considering a patient's anatomy. The general framework of using automated reconstruction, big data, and statistical methods to investigate structure-function relationships may be used in many biomedical contexts.

Our analysis provides the following insights in how sex-related anatomical differences affected the impact of myocardial infarction on key ECG biomarkers. 1) Smaller cavity volumes are associated with approximately half of the shorter QRS durations in females than males in both healthy and post-MI subjects. 2) Female STJ amplitude is lower than male in all precordial leads for healthy and post-MI subjects, associated with a smaller LV mass and more superior and posterior position. 3) Female TWA changes following MI are more associated with anatomical factors than male. 4) R axis is more left deviated in MI than healthy; for females this is associated with a more horizontal cardiac long axis, but for males with electrophysiology.

The high Dice coefficient for the contour extraction and low surface-to-contour distances show that the extracted contours are near the ground truth torso-air boundary on the clinical imaging, as well as to the final reconstructed surfaces. As detailed in Smith et al. [40], the three-step segmentation, automated post-processing, and refinement process was particularly effective at removing errors inside the torso at locations of sharp gradient between dark and light, for example due to air in the lungs. Whilst reconstructed 3D torso surfaces were largely smooth and realistic, there were small irregularities, generally on the shoulder and waist regions. These were not typically associated with incomplete CMR artifact removal and may instead result from images being taken on different breath-holds or the image sparsity. The low surface-to-surface distance between reconstructions made using the automatically and manually derived contours demonstrates that the small errors in contour extraction did not lead to significant errors in electrode placement on the torso meshes. Surfaces were generally more accurate on the upper left quadrant of the torso, which is where most electrodes are placed. The validity of the torso-ventricular reconstruction pipeline is further supported as known trends in torso and cardiac size, position, and orientation were qualitatively reproduced, and furthermore were quantitatively characterised. This includes the more superior female cardiac position [13, 41] and the horizontal shift in the cardiac long axis for subjects with a larger BMI [32, 34, 35]. As this pipeline uses clinically standard CMR imaging, it can be more easily translated to a clinical tool to correct for the effect of anatomical variation on the ECG in a variety of medical contexts.

QRS duration and its dispersion have been a key component of proposed electrocardiographic risk stratification for SCD following MI. However, findings of its effectiveness are mixed, with some trials suggesting it is a predictor of arrhythmic risk following MI [28, 29], but others finding that it is more likely a predictor of general mortality than arrhythmic inducibility [42, 43]. Our finding of QRS prolongation in post-MI subjects is consistent with previous studies finding increased QRS duration in the acute stages post-MI, particularly cooccurring with ST changes in leads exploring the infarcted

region [7]. This prolongation has been shown to increase over time in the months following infarct for patients with LV dysfunction [44]. It is associated with slowed conduction velocity in the infarcted region itself, involvement of the conduction system such as the bundle branches and Purkinje, and in the chronic case, with dilation and hypertrophy of non-infarcted myocardium [42, 44-47]. Both clinically prolonged, defined as >120ms in bundle branch block, and moderately prolonged QRS durations have been associated with increased risk following MI [48, 49]. We found that even small differences in the QRS duration are significant in the context of risk stratification, as in lead aVL, mean female QRS duration would have to increase by 27% more than male to exceed 120ms and by 68% more to exceed 100ms. The combination of increased TWA and QRS prolongation in the septal leads from electrophysiology for females may specifically point to hypertrophy or remodelling of the calcium channels in the septum. However, this may be missed if structure were not accounted for, particularly as structural changes mask the septal TWA increase. Our finding that QRS duration is consistently related to cardiac orientation, particularly for healthy subjects, is broadly in line with simulation studies [2], but goes further to characterise trends across large populations and between demographic groups. The increased sensitivity of QRS duration to cardiac orientation for healthy, compared with post-MI, subjects may be explained by the deformation of the depolarisation wave's path through the myocardium for infarcted patients by areas of reduced electrical activity [45]. This creates a different projection of the QRS vector to each lead axis. Our finding that QRS duration is positively associated with cardiac size is in line with both previous simulation studies [1], and with the biophysical understanding that larger distances require longer to traverse [6]. However, the estimation of the proportion of sex differences associated with structural variation is striking. This suggests that if demographic characteristics that impact anatomy, particularly sex, are taken into account as proxies for those anatomical differences, corrected QRS duration and parameters related to it may be more representative of the underlying electrophysiological changes that predispose post-MI patients to SCD. This may therefore improve its accuracy in risk stratification, without the need for CMR imaging.

The finding that STJ amplitude was substantially lower in females than males in all septal and anterior leads (V1-V4) is striking. The ECG data was not from subjects undergoing myocardial infarctions, so is instructive in sex differences in the normal baseline of STJ amplitude, from which any deviations can be measured, not in the changes to that baseline in acute infarction. The Fourth Universal Definition of Myocardial Infarction only has sex-specific thresholds in leads V2 and V3 for identifying ST-elevation, a key component in the diagnosis of ST-elevated myocardial infarctions (STEMIs), whereas in other leads, the threshold is the same for both sexes [14]. The dual effects of cardiac and torso volume necessitate the interpretation of ST-elevation through the lens of the anatomical context of the patient. For example, in lead V4, the clinical threshold for both female and male ST-elevation is 0.1mV [14]. However, due to their previously stated lower baseline values, overweight healthy females would have to have a 63% larger increase in STJ amplitude to be classified as ST-elevated than normal weight healthy males. This is a critical observation in the context of higher incidence of missed diagnosis and increased female MI mortality in both the short and longer term following the event [19, 22, 23]. Previous studies performed on the cardiac structure-function relationship did not investigate the STJ amplitude [1, 2], though the effect of cardiac positioning has been noted experimentally from changes to STJ amplitude caused by differences in body posture [50]. Therefore, this work represents a significant step forward in the characterisation of anatomical influences of its baseline level, from which deviations can then be more accurately identified in the context of anatomical variation. It also highlights the important intersectional effects of demographic characteristics such as sex and BMI, suggesting that both of

these factors should be accounted for in assessing ST-elevation to improve accuracy of MI diagnosis and classification.

Changes in TWA are particularly clinically relevant in MI. Firstly, alterations to the polarity and amplitude of the T wave are used in diagnosis of acute MI [14]. Secondly, TWA affects measures proposed for use in risk stratification following MI, particularly markers of repolarisation abnormalities such as the spatial ventricular gradient, and for assessing the infarct size electrocardiographically [26, 51]. Acutely, hyperkalaemia can lead to hyperacute T waves [52, 53], and repolarisation heterogeneities to T wave inversion [54]. However, in the progression to chronic MI, reductions in L-type calcium and sodium currents [55, 56] can both cause TWA reductions [57, 58]. The latter effects are captured in the electrophysiological contributions to TWA reduction in Figures 4E and 4F. However, particularly in the female case, a substantial proportion of TWA changes are associated with anatomical differences, such as the decreased verticality of the post-MI heart. This implies that without anatomical corrections, such as adjusting for BMI, the female TWA may be less representative of its underlying electrophysiology, and therefore less representative of any pathology. This increased effect of anatomical parameters in females is broadly related to two factors. Firstly, the difference in key anatomical factors such as posterior position and long axis orientation from healthy to post-MI subjects is larger in females. This reflects their larger increase in BMI, as a larger BMI was associated with a more horizontal cardiac long axis, consistent with previous works that suggested this was related to an upwards shift in the diaphragm [32, 35]. The female TWA can also be more sensitive to changes in anatomical parameters, for example the increased sensitivity to the cardiac long axis angle in the inferior leads. This could be explained by sex differences in the directions of the T wave vectors and nonlinearities in the structure-function relationships. Our finding that TWA is affected by cardiac position and orientation is in line with previous simulation studies [2], and with the physical understanding that amplitude increases with decreased distance to the electrode and better alignment between the lead axes and electrical vectors. However, while their small number of anatomies (N=5) limited their conclusions to these relationships being significant but patient dependent, the vast increase in anatomies that our work considered (N=1476) facilitated more specific characterisations of population and demographic trends. This demonstrates the power of automated, high-throughput anatomical reconstruction to ensure that electrophysiological parameters are equally representative of underlying pathology in females and males.

Electrical axes are fundamental to certain ECG parameters proposed to stratify arrhythmic risk post-MI, particularly markers of electrical heterogeneity such as QRS-T angle [59]. However, the relationship between electrical and anatomical axes is complex and poorly understood, with previous works on smaller populations even disagreeing over whether there was any significant relationship between the two [32, 60, 61]. Our finding that the verticality of the cardiac long axis is particularly significant in determining R axis angle, especially for females, represents a step forward in understanding this relationship. Moreover, our work finds that while the left-deviation of the R axis may look similar in both sexes, in males this is representative of an electrophysiological change, presumably alterations to the direction of the QRS vector caused by both hypertrophy and areas of electrical inactivity. However, for females this change is almost entirely associated with anatomical differences. This suggests that it is particularly important to correct R axis angles for anatomical factors in females to avoid misattribution of deviations to electrophysiological pathology. The significant relationship between torso volume and R axis angle for healthy subjects indicates that BMI may be a critical consideration when using ECG based biomarkers that are sensitive to axis angles. The fact that increased torso volume moved the LL electrode further away from the heart centre than the LA electrode suggests that this relationship is caused by a stretching of the

anatomical plane in which these angles are viewed. This relationship was not present in post-MI subjects, which may be related to their different body shapes, specifically larger BMIs, and a higher prevalence of central obesity [62], and again to the different electrical path that the QRS vector takes in infarcted ventricles. Therefore, this represents another area in which a clinical tool that accounts for anatomical variation in interpreting ECG biomarkers would reduce differential accuracy in risk stratification between demographic groups.

Due to the demographics of the UK Biobank [38], this study only included subjects aged 45-80 years old; however, the incidence of MI is very low in people younger than this range [23]. The ethnic background of the dataset also had limited diversity; however, this is roughly representative of the UK Biobank population, which itself approximately represented the ethnic composition of the UK at the time of recruitment [63]. As these databases become more diverse, the mediating effect of ethnic background on the cardiac structure-function relationship should be investigated. Whilst the healthy subjects had a roughly equal sex balance, the post-MI subjects had a male-female ratio of approximately 4:1. This is however in line with sex differences in diagnosed MI events in the UK [64]. The statistical shape model used for initial torso reconstruction did not have separate male and female models, which may have led to an underestimation in the sex differences in the torsos of male and female anatomies. However, the deformation step of the torso surface towards the contours was designed to address this issue by modelling personalised torso variations. The coverage of the contours from the clinical CMR images is sparse, and there are areas on the torso where there is little correction from the deformation step. However, this is mainly in the lower abdomen and right-hand side of the chest, which is distant from most of the electrode positions. The exact electrode positions of the obtained ECGs were not available in the UK Biobank dataset, so these were estimated by placing the electrodes on standard positions on the personalised torso. However, this estimation process allows for use of many similar clinically standard datasets, avoiding complex acquisition protocols. As the anatomical factors cannot represent a perfectly complete and independent basis set, the electrophysiological contribution can only be estimated. However as there is more anatomical variation than can be represented using the given factors, such as the smaller scale geometry of the heart, the role of the anatomy versus electrophysiology was likely under- rather than overestimated. Whilst the study benefits from the electrophysiological and anatomical variation that using clinical data facilitates, it is impossible to fully separate the effects of these factors on ECG biomarkers, as characteristics such as sex affect both categories, making them interdependent. This means that this work complements both previous and future computational studies, which have less interpersonal variability, but isolate the effect of positional and rotational changes. Future work should focus on the characterisation of ECG biomarkers in myocardial infarction and other disease conditions. The automated torso reconstruction pipeline this work proposes enables the expansion of the number of anatomies such future computational studies would investigate.

In this work, we have developed a fully automated pipeline for personalised torso reconstruction, by first extracting the torso contours from standard clinical CMR images and then generating a 3D torso reconstruction from the series of 2D contours. The interplay between torso-ventricular anatomy, ECG biomarkers, and demographic characteristics, such as sex, was analysed for 1051 healthy, and 425 post-MI, subjects. For females, anatomical differences in post-MI compared with healthy subjects, such as a more horizontal cardiac long axis and more posterior cardiac position, contributed more to their reduced TWA and left deviated R axis. However, for males, their corresponding post-MI ECG changes were more reflective of electrophysiological differences. Female STJ amplitude was significantly lower than male, partly due to their reduced left ventricular mass and differences in cardiac position. This has particularly relevant implications in diagnosing high-risk

MI events. Approximately half of the decreased QRS duration in females, compared with males, was associated with their decreased cavity volume, highlighting the significance of the role of anatomical versus electrophysiological causes of interpersonal variation. This underlines the importance of, and lays the foundations for, personalised ECG interpretation that considers a subject's individual torso-ventricular anatomy, facilitating improvement in diagnosis and risk stratification tools.

Materials and methods

Dataset

The UK Biobank (UKB) dataset [38] was chosen for its high quality CMR imaging and 12-lead ECGs, along with demographic and disease information. The UKB cohort includes both healthy subjects and those with a range of cardiovascular and other diseases. For the 3D torso reconstruction, only the scout MR images were selected for heart scans. For each subject, approximately 60 images were found. A random sample of 100 subjects was chosen to train the torso contour extraction network. A further 30 subjects, selected to be representative of the demographics of the dataset, as described in Section 1.1 of the Supplementary Materials, were chosen to act as an independent test set.

For the 3D torso reconstruction, 1646 control subjects were randomly selected from the UKB cohort alongside 479 subjects with a history of MI. MI was defined as any history of MI including ST- and non-ST-elevation MI, as obtained from patients' self-report in the baseline questionnaire and nurse-led interview, and linked hospital admission data [65]. From the 1646 controls, 3 cases were excluded for incomplete image sets, and 592 were excluded for having at least one of 82 disease diagnoses in their UKB records, including circulatory system, renal, genitourinary, and endocrine disorders. The final set included 1051 'healthy' controls (581 female and 470 male), as shown in the left panel of Supplemental Figure 1. From the 479 post-MI subjects, 6 were excluded for incomplete image sets, 13 for missing ECG data, and 35 were excluded due to their imaging occurring before the MI event, thus retaining 425 post-MI subjects (84 female and 341 male), as shown in the right panel of Supplemental Figure 1. 92.7% of subjects identified as White British. No statistically significant difference was observed between the two subpopulations in terms of ethnicity. Mean age was 61.1 ± 7.5 years for the healthy population and 67.3 ± 6.2 years for post-MI patients, and likewise mean BMI was 25.9 ± 4.1 kg/m² and 28.1 ± 4.4 kg/m², respectively. Demographic characteristics of both subpopulations are shown in Table 1.

Contour extraction

Whilst the CMR images are of high quality and have been collected using a clinically standard procedure, they aim at imaging of the heart and not the torso. This presents several problems for torso reconstruction, as addressed in Smith et al. [40]. In order to automatically and accurately extract the torso boundaries, the proposed contour extraction task was partitioned into three stages. Firstly, a segmentation network was trained to achieve a binary mask across all visible sections of the body. Secondly, automated post-processing was applied to extract the largest single continuous contour on the binary mask, removing any contour inside the body or anatomy separate from the torso. Thirdly, a refinement network was trained to remove any sections of the contour due to unwanted anatomical features such as the head, neck and connected sections of the arms, and any boundary caused by an MRI artifact.

U-Net [66] was chosen for the architecture of both networks, due to its extensive success in MRI segmentation tasks [67, 68]. Implementation of both network architectures are described in Smith et al. [40].

Manual segmentations of the CMR images were performed using a proprietary graphical user interface tool written in MATLAB. 15 subjects (891 individual images) were annotated to be used in the segmentation network, and likewise 100 subjects (5993 individual images) were annotated for the refinement network. A random sample of 30 subjects representing the diverse UK Biobank demography was contoured to be used as an independent test set. Both networks were trained using a five-fold cross validation framework, and the optimum network was chosen based on Dice coefficient, Hausdorff distance, and qualitative results. The loss function used was Dice loss, and the optimiser was Adam [69]. Final results were compared using the three-stage segmentation, post-processing, and refinement pipeline, previously described, with using a similar single U-Net architecture to process the raw image directly to the refined contour.

Reconstruction

To generate the initial 3D torso mesh, a statistical shape model (SSM) was applied over the automatically extracted sparse torso contours in 3D space, which was then optimally deformed by minimising the distance to the extracted contours to produce the final 3D torso mesh.

Fitting the SSM

In order to generate the torso meshes from the sparse torso contours, a high-resolution statistical shape model (SSM) of human body shapes, was employed for the initial 3D torso reconstruction. The SSM was generated from the 3D optical body surface scanning of 4308 subjects in the CAESAR study, the largest commercially available scan database to date [70]. Detailed information on the SSM generation is provided in [71]. As the initial condition, the mean SSM was translated into the subject's coordinate system by positioning the centre of heart from the mean SSM onto the centre of the subject's heart. The latter centre was approximated by the closest point to the intersection lines between the cine short axis (SAX) and long axis (LAX) slices. Over the automatically extracted sparse torso contours in 3D space, the SSM was fitted by the optimal estimation of principal components, followed by rigid transformation, such that:

$$\min_{q,R} \sum_i d(C_i, R(\bar{X} + \Phi q))^2$$

where C_i is the i^{th} point on sparse torso representation, \bar{X} the mean shape model, $\Phi = (\phi_1, \phi_2, \dots)$ the SSM modes of variations, q the estimated set of parameters along the principal modes, and R the rigid transformation. The fitting of the reconstructions was restricted to the first 40 principal components of the SSM.

Deforming for patient-specific torso reconstruction

The initial generated torso mesh is inherently limited by the variability in the SSM. Hence, in order to accurately capture subject-specific variations, a final deformation step was performed via approximate thin plate splines (TPS) [72] to produce the final 3D torso mesh, minimising the distance to the extracted contours. In case the automated torso contour extraction generated sparse outlier points, any torso points over the 95th percentile were removed.

The initial deformation field was computed by considering the closest point on the SSM-generated mesh from the points on the sparse representation. A series of small, smooth deformations using approximate TPS was then applied to push the 3D mesh closer to the torso points, while preserving the smoothness and local topological properties [73]. Let F be the deformation field such that:

$$\arg \min_F \lambda \sum_i (\|F(P_i) - Q_i'\|)^2 + J_2^3(F) \text{ and } Q_i' = P_i + \beta \frac{(Q_i - P_i)}{\|Q_i - P_i\|}$$

where $\{P_i\}$ is the set of closest points on the surface M_t to the torso points $\{Q_i\}$ on the sparse model, and J_2^3 is the TPS functional using derivatives of order 2 and image dimensions 3. The deformation $M_{t+1} = F(M_t)$ was iteratively applied in a diffeomorphic manner, resulting in a composition of several smooth approximations approaching initial mesh M towards the sparse representation. Laplacian smoothing, decimation, and affine transformation were applied in the end to ensure the local geometric and topological characteristics of the reconstructed mesh. Finally, the torso surface was remeshed with a restricted Frontal-Delaunay algorithm using the mesh generator JIGSAW [74] with a specified element size of 1cm.

Extraction of anatomical biomarkers

Torso reconstructions were manually inspected to ensure that they did not include any of the subject's head or extraneous sections of the arm. The torso volume was calculated using PyVista [75], as the volume enclosed by the reconstructed torso surface. The 3D heart mesh was reconstructed from cine MR slices using the automated pipeline presented in [76]. The locations of the ECG electrodes (V1-V6, LA, RA, LL, RL) were identified on the mean SSM torso, and their positions were transformed with the mesh such that the resulting personalised mesh had electrodes located in equivalent locations relative to the new torso shape.

The x position (lateral) of the heart relative to the ECG electrodes was determined by setting the location of the most rightward electrode on the body as $x = 0$ and the most leftward as $x = 1$ and noting the position of the centre of the heart along this scale. y (posterior) and z (superior) positions were found similarly by setting the most frontward electrode as $y = 0$, backward as $y = 1$, downward as $z = 0$, and upward as $z = 1$. For estimating the heart position, the intersection point of the LAX four-chamber plane, LAX two-chamber plane, and the middle slice of the SAX stack was identified. For estimating the heart orientation, the X-axis was first measured in the cardiac system as the intersecting line between the LAX four-chamber plane and the mid SAX slice, while the Z-axis was identified as the perpendicular line to the X-axis that passed through the LAX four-chamber plane. The Y-axis was estimated as the normal to the XZ-plane. For calculating the Euler angles (α , β , γ), as shown in Figure 1, the intersecting line, denoted as x' , between the XY-plane in the cardiac system and the xy-plane in the real (torso) coordinate system was first identified. α was measured as the angle between the x-axis in the real system and the intersecting line x' , essentially presenting the spin of the XY-plane around the z-axis. The γ angle was calculated as the angle between the X-axis in the cardiac system and the intersecting line, i.e., the tilt of the X-axis with respect to the xy-plane. β was measured as the angle between the Z-axis in the cardiac system and the z-axis in the real (torso) system, i.e., the verticality of the cardiac long axis. The calculations of the coordinate systems and angles are presented in lower-left corner of Figure 1.

Reconstruction validation

In order to evaluate the performance of the contour extraction procedure, reconstructions of 30 subjects were made using the fully automated pipeline. These were compared with reconstructions made using manually annotated contours. A ray tracing method [77] was applied to obtain the distance between 3D torso surfaces. For each point on one surface, the normal to the surface was found, and the nearest intersection between that line and the second surface (in either direction) was obtained. Since the normal is not guaranteed to intersect the surface or may intersect at a point on the opposing side of the torso, the nearest neighbouring point on the second surface was also found for each point. The minimum between these two distances was taken for each point as the surface-to-surface distance. The distance between each electrode location on the different torsos was also taken as a measure of similarity for the reconstructions. The mean surface-to-contour distance was calculated for each test subject to evaluate the quality of the reconstruction.

Statistical analysis

Split violin plots were created to show distributions of anatomical and ECG biomarkers, and are shown in Supplemental Figures 2 and 3. STJ amplitude refers to the amplitude of the ST segment measured at the J point (the end of the QRS complex). Mean values of all biomarkers were compared between healthy and post-MI subjects of either sex, and male and female subjects of either MI status. The Shapiro-Wilk test was used to ascertain whether both subpopulations had a normal distribution. If there was significant evidence of non-normality, the Wilcoxon test was used. The Levene test was used to determine whether the subpopulations had an equal variance. If there was sufficient evidence of nonequal variance, the Welch's *t*-test was used, otherwise, the standard *t*-test was used.

Linear regression models were created relating ECG biomarkers with anatomical factors. As the two measures of cardiac size (total cavity volume and left ventricular mass) were highly colinear, one was selected for each ECG biomarker depending on the minimisation of mean Akaike information criterion (AIC) across the 12 leads. Regression coefficients were normalised by the standard deviation of both the dependent and independent variables to allow for easy comparison. To estimate the contribution of each factor to the difference in key ECG biomarkers from females to males and from healthy to post-MI subjects, the raw regression coefficients for each factor were multiplied by the overall difference in that ECG biomarker. The contribution of electrophysiology to sex and MI status differences was estimated as the remaining difference after all anatomical factors had been accounted for.

References

- 1 Mincholé, A., Zacur, E., Ariga, R., Grau, V., and Rodriguez, B.: 'MRI-Based Computational Torso/Biventricular Multiscale Models to Investigate the Impact of Anatomical Variability on the ECG QRS Complex', *Front Physiol*, 2019, 10
- 2 Nguyễn, U.C., Potse, M., Regoli, F., Caputo, M.L., Conte, G., Murzilli, R., Muzzarelli, S., Moccetti, T., Caiani, E.G., Prinzen, F.W., Krause, R., and Auricchio, A.: 'An in-silico analysis of the effect of heart position and orientation on the ECG morphology and vectorcardiogram parameters in patients with heart failure and intraventricular conduction defects', *Journal of Electrocardiology*, 2015, 48, (4), pp. 617-625
- 3 MacLeod, R.S., Ni, Q., Punske, B., Ershler, P.R., Yilmaz, B., and Taccardi, B.: 'Effects of heart position on the body-surface electrocardiogram', *Journal of Electrocardiology*, 2000, 33, pp. 229-237
- 4 Bradley, C.P., Pullan, A.J., and Hunter, P.J.: 'Effects of Material Properties and Geometry on Electrocardiographic Forward Simulations', *Annals of Biomedical Engineering*, 2000, 28, (7), pp. 721-741
- 5 Hoekema, R., Uijen, G.J.H., and Oosterom, A.v.: 'Geometrical aspects of the interindividual variability of multilead ECG recordings', *IEEE Transactions on Biomedical Engineering*, 2001, 48, (5), pp. 551-559
- 6 van Oosterom, A., Hoekema, R., and Uijen, G.J.H.: 'Geometrical factors affecting the interindividual variability of the ECG and the VCG', *Journal of Electrocardiology*, 2000, 33, pp. 219-227
- 7 Chávez-González, E., Jiménez, A.R., and Moreno-Martínez, F.: 'QRS duration and dispersion for predicting ventricular arrhythmias in early stage of acute myocardial infraction', *Medicina Intensiva (English Edition)*, 2017, 41, (6), pp. 347-355

- 8 Kittnar, O.: 'Sex Related Differences in Electrocardiography', *Physiological Research*, 2023, 72
- 9 Prajapati, C., Koivumäki, J., Pekkanen-Mattila, M., and Aalto-Setälä, K.: 'Sex differences in heart: from basics to clinics', *European Journal of Medical Research*, 2022, 27, (1), pp. 241
- 10 Daniels, S.R., Kimball, T.R., Morrison, J.A., Khoury, P., Witt, S., and Meyer, R.A.: 'Effect of Lean Body Mass, Fat Mass, Blood Pressure, and Sexual Maturation on Left Ventricular Mass in Children and Adolescents', *Circulation*, 1995, 92, (11), pp. 3249-3254
- 11 Kansal, S., Roitman, D., and Sheffield, L.: 'A quantitative relationship of electrocardiographic criteria of left ventricular hypertrophy with echocardiographic left ventricular mass: a multivariate approach', *Clin Cardiol*, 1983, 6, (9), pp. 456-463
- 12 Gambill, C.L., Wilkins, M.L., Haisty, W.K., Anderson, S.T., Maynard, C., Wagner, N.B., Startt Selvester, R.H., and Wagner, G.S.: 'T wave amplitudes in normal populations: Variation with ECG lead, sex, and age', *Journal of Electrocardiology*, 1995, 28, (3), pp. 191-197
- 13 Güneş Bolatlı, N.Ü., Mustafa Koplay, Zeliha Fazlıoğulları, Ahmet Kağan Karabulut: 'Examination of the levels of structures in the thorax in multidetector computerized tomography images', *Journal of Surgery and Medicine*, 2020, 4, (9), pp. 784-789
- 14 Thygesen, K., Alpert, J.S., Jaffe, A.S., Chaitman, B.R., Bax, J.J., Morrow, D.A., White, H.D., and Group, E.S.C.S.D.: 'Fourth universal definition of myocardial infarction (2018)', *European Heart Journal*, 2019, 40, (3), pp. 237-269
- 15 Collet, J.-P., Thiele, H., Barbato, E., Barthélémy, O., Bauersachs, J., Bhatt, D.L., Dendale, P., Dorobantu, M., Edvardsen, T., Folliguet, T., Gale, C.P., Gilard, M., Jobs, A., Jüni, P., Lambrinou, E., Lewis, B.S., Mehilli, J., Meliga, E., Merkely, B., Mueller, C., Roffi, M., Rutten, F.H., Sibbing, D., Siontis, G.C.M., Chettibi, M., Hayrapetyan, H.G., Metzler, B., Najafov, R., Stelmashok, V.I., Claeys, M., Kušljugić, Z., Gatzov, P.M., Skoric, B., Panayi, G., Mates, M., Sorensen, R., Shokry, K., Marandi, T., Kajander, O.A., Commeau, P., Aladashvili, A., Massberg, S., Nikas, D., Becker, D., Guðmundsdóttir, I.J., Peace, A.J., Beigel, R., Indolfi, C., Aidargaliyeva, N., Elezi, S., Beishenkulov, M., Maca, A., Gustiene, O., Degrell, P., Cassar Maempel, A., Ivanov, V., Damman, P., Kedev, S., Steigen, T.K., Legutko, J., Morais, J., Vinereanu, D., Duplyakov, D., Zavatta, M., Pavlović, M., Orban, M., Bunc, M., Ibañez, B., Hofmann, R., Gaemperli, O., Marjeh, Y.B., Addad, F., Tutar, E., Parkhomenko, A., Karia, N., and Group, E.S.C.S.D.: '2020 ESC Guidelines for the management of acute coronary syndromes in patients presenting without persistent ST-segment elevation: The Task Force for the management of acute coronary syndromes in patients presenting without persistent ST-segment elevation of the European Society of Cardiology (ESC)', *European Heart Journal*, 2021, 42, (14), pp. 1289-1367
- 16 Ibanez, B., James, S., Agewall, S., Antunes, M.J., Bucciarelli-Ducci, C., Bueno, H., Caforio, A.L.P., Crea, F., Goudevenos, J.A., Halvorsen, S., Hindricks, G., Kastrati, A., Lenzen, M.J., Prescott, E., Roffi, M., Valgimigli, M., Varenhorst, C., Vranckx, P., Widimský, P., and Group, E.S.C.S.D.: '2017 ESC Guidelines for the management of acute myocardial infarction in patients presenting with ST-segment elevation: The Task Force for the management of acute myocardial infarction in patients presenting with ST-segment elevation of the European Society of Cardiology (ESC)', *European Heart Journal*, 2018, 39, (2), pp. 119-177
- 17 Bugiardini, R., and Cenko, E.: 'Sex differences in myocardial infarction deaths', *The Lancet*, 2020, 396, (10244), pp. 72-73
- 18 Brush, J.E., Krumholz, H.M., Greene, E.J., and Dreyer, R.P.: 'Sex Differences in Symptom Phenotypes Among Patients With Acute Myocardial Infarction', *Circulation: Cardiovascular Quality and Outcomes*, 2020, 13, (2), pp. e005948
- 19 Pope, J.H., Aufderheide, T.P., Ruthazer, R., Woolard, R.H., Feldman, J.A., Beshansky, J.R., Griffith, J.L., and Selker, H.P.: 'Missed diagnoses of acute cardiac ischemia in the emergency department', *New England Journal of Medicine*, 2000, 342, (16), pp. 1163-1170
- 20 Chandra, N.C., Ziegelstein, R.C., Rogers, W.J., Tiefenbrunn, A.J., Gore, J.M., French, W.J., Rubison, M., and for the National Registry of Myocardial Infarction, I.: 'Observations of the

Treatment of Women in the United States With Myocardial Infarction: A Report From the National Registry of Myocardial Infarction-I', *Archives of Internal Medicine*, 1998, 158, (9), pp. 981-988

21 Bairey Merz, C.N., Shaw Leslee, J., Reis Steven, E., Bittner, V., Kelsey Sheryl, F., Olson, M., Johnson, B.D., Pepine Carl, J., Mankad, S., Sharaf Barry, L., Rogers William, J., Pohost Gerald, M., Lerman, A., Quyyumi Arshed, A., Sopko, G., and null, n.: 'Insights From the NHLBI-Sponsored Women's Ischemia Syndrome Evaluation (WISE) Study', *Journal of the American College of Cardiology*, 2006, 47, (3_Supplement), pp. S21-S29

22 Fang, J., Alderman, M.H., Keenan, N.L., and Ayala, C.: 'Acute Myocardial Infarction Hospitalization in the United States, 1979 to 2005', *The American Journal of Medicine*, 2010, 123, (3), pp. 259-266

23 Benjamin, E.J., Muntner, P., Alonso, A., Bittencourt, M.S., Callaway, C.W., Carson, A.P., Chamberlain, A.M., Chang, A.R., Cheng, S., Das, S.R., Delling, F.N., Djousse, L., Elkind, M.S.V., Ferguson, J.F., Fornage, M., Jordan, L.C., Khan, S.S., Kissela, B.M., Knutson, K.L., Kwan, T.W., Lackland, D.T., Lewis, T.T., Lichtman, J.H., Longenecker, C.T., Loop, M.S., Lutsey, P.L., Martin, S.S., Matsushita, K., Moran, A.E., Mussolino, M.E., O'Flaherty, M., Pandey, A., Perak, A.M., Rosamond, W.D., Roth, G.A., Sampson, U.K.A., Satou, G.M., Schroeder, E.B., Shah, S.H., Spartano, N.L., Stokes, A., Tirschwell, D.L., Tsao, C.W., Turakhia, M.P., VanWagner, L.B., Wilkins, J.T., Wong, S.S., Virani, S.S., and null, n.: 'Heart Disease and Stroke Statistics—2019 Update: A Report From the American Heart Association', *Circulation*, 2019, 139, (10), pp. e56-e528

24 Coventry, L.L., Finn, J., and Bremner, A.P.: 'Sex differences in symptom presentation in acute myocardial infarction: A systematic review and meta-analysis', *Heart & Lung*, 2011, 40, (6), pp. 477-491

25 Shaw Leslee, J., Bairey Merz, C.N., Pepine Carl, J., Reis Steven, E., Bittner, V., Kelsey Sheryl, F., Olson, M., Johnson, B.D., Mankad, S., Sharaf Barry, L., Rogers William, J., Wessel Timothy, R., Arant Christopher, B., Pohost Gerald, M., Lerman, A., Quyyumi Arshed, A., Sopko, G., and null, n.: 'Insights From the NHLBI-Sponsored Women's Ischemia Syndrome Evaluation (WISE) Study', *Journal of the American College of Cardiology*, 2006, 47, (3_Supplement), pp. S4-S20

26 Bui, A.H., and Waks, J.W.: 'Risk Stratification of Sudden Cardiac Death After Acute Myocardial Infarction', *J Innov Card Rhythm Manag*, 2018, 9, (2), pp. 3035-3049

27 Dagues, N., and Hindricks, G.: 'Risk stratification after myocardial infarction: is left ventricular ejection fraction enough to prevent sudden cardiac death?', *European Heart Journal*, 2013, 34, (26), pp. 1964-1971

28 Dhar, R., Alsheikh-Ali, A.A., Estes, N.A.M., Moss, A.J., Zareba, W., Daubert, J.P., Greenberg, H., Case, R.B., and Kent, D.M.: 'Association of prolonged QRS duration with ventricular tachyarrhythmias and sudden cardiac death in the Multicenter Automatic Defibrillator Implantation Trial II (MADIT-II)', *Heart Rhythm*, 2008, 5, (6), pp. 807-813

29 Zimetbaum, P.J., Buxton, A.E., Batsford, W., Fisher, J.D., Hafley, G.E., Lee, K.L., O'Toole, M.F., Page, R.L., Reynolds, M., and Josephson, M.E.: 'Electrocardiographic Predictors of Arrhythmic Death and Total Mortality in the Multicenter Unsustained Tachycardia Trial', *Circulation*, 2004, 110, (7), pp. 766-769

30 Waks, J.W., and Tereshchenko, L.G.: 'Global electrical heterogeneity: A review of the spatial ventricular gradient', *Journal of Electrocardiology*, 2016, 49, (6), pp. 824-830

31 Oehler, A., Feldman, T., Henrikson, C.A., and Tereshchenko, L.G.: 'QRS-T Angle: A Review', *Annals of Noninvasive Electrocardiology*, 2014, 19, (6), pp. 534-542

32 Sathanathan, G., Aggarwal, G., Zahid, S., Byth, K., Chik, W., Friedman, D., and Thiagalingam, A.: 'Computed tomography-guided in vivo cardiac orientation and correlation with ECG in individuals without structural heart disease and in age-matched obese and older individuals', *Clinical Anatomy*, 2015, 28, (4), pp. 487-493

33 Sang, Y., Beetz, M., and Grau, V.: 'Generation of 12-Lead Electrocardiogram with Subject-Specific, Image-Derived Characteristics Using a Conditional Variational Autoencoder', in Editor

- (Ed.)^(Eds.): 'Book Generation of 12-Lead Electrocardiogram with Subject-Specific, Image-Derived Characteristics Using a Conditional Variational Autoencoder' (2022, edn.), pp. 1-5
- 34 Rautaharju, P.M., Zhou, S.H., and Calhoun, H.P.: 'Ethnic differences in ECG amplitudes in North American white, black, and Hispanic men and women: Effect of obesity and age', *Journal of Electrocardiology*, 1994, 27, pp. 20-31
- 35 Engblom, H., Hedström, E., Palmer, J., Wagner, G.S., and Arheden, H.: 'Determination of the left ventricular long-axis orientation from a single short-axis MR image: relation to BMI and age', *Clinical Physiology and Functional Imaging*, 2004, 24, (5), pp. 310-315
- 36 Yusuf, S., Hawken, S., Öunpuu, S., Bautista, L., Franzosi, M.G., Commerford, P., Lang, C.C., Rumboldt, Z., Onen, C.L., Lisheng, L., Tanomsup, S., Wangai, P., Jr., Razak, F., Sharma, A.M., and Anand, S.S.: 'Obesity and the risk of myocardial infarction in 27 000 participants from 52 countries: a case-control study', *The Lancet*, 2005, 366, (9497), pp. 1640-1649
- 37 Piro, M., Della Bona, R., Abbate, A., Biasucci Luigi, M., and Crea, F.: 'Sex-Related Differences in Myocardial Remodeling', *Journal of the American College of Cardiology*, 2010, 55, (11), pp. 1057-1065
- 38 Petersen, S.E., Matthews, P.M., Bamberg, F., Bluemke, D.A., Francis, J.M., Friedrich, M.G., Leeson, P., Nagel, E., Plein, S., Rademakers, F.E., Young, A.A., Garratt, S., Peakman, T., Sellors, J., Collins, R., and Neubauer, S.: 'Imaging in population science: cardiovascular magnetic resonance in 100,000 participants of UK Biobank - rationale, challenges and approaches', *Journal of Cardiovascular Magnetic Resonance*, 2013, 15, (1), pp. 46
- 39 Dougherty, J.D.: 'The relation of the frontal QRS axis to the anatomic position of the heart', *Journal of Electrocardiology*, 1970, 3, (3), pp. 267-284
- 40 Smith, H.J., Banerjee, A., Choudhury, R.P., and Grau, V.: 'Automated Torso Contour Extraction from Clinical Cardiac MR Slices for 3D Torso Reconstruction', in Editor (Ed.)^(Eds.): 'Book Automated Torso Contour Extraction from Clinical Cardiac MR Slices for 3D Torso Reconstruction' (2022, edn.), pp. 3809-3813
- 41 Mirjalili, S.A., Hale, S.J.M., Buckenham, T., Wilson, B., and Stringer, M.D.: 'A reappraisal of adult thoracic surface anatomy', *Clinical Anatomy*, 2012, 25, (7), pp. 827-834
- 42 Yerra, L., Anavekar, N., Skali, H., Zelenkofske, S., Velazquez, E., McMurray, J., Pfeffer, M., and Solomon, S.D.: 'Association of QRS duration and outcomes after myocardial infarction: the VALIANT trial', *Heart Rhythm*, 2006, 3, (3), pp. 313-316
- 43 Buxton Alfred, E., Sweeney Michael, O., Wathen Mark, S., Josephson Mark, E., Otterness Mary, F., Hogan-Miller, E., Stark Alice, J., DeGroot Paul, J., and null, n.: 'QRS Duration Does Not Predict Occurrence of Ventricular Tachyarrhythmias in Patients With Implanted Cardioverter-Defibrillators', *Journal of the American College of Cardiology*, 2005, 46, (2), pp. 310-316
- 44 Brembilla-Perrot, B., Houriez, P., Claudon, O., Preiss, J.-P., and De La Chaise, A.T.: 'Evolution of QRS Duration after Myocardial Infarction: Clinical Consequences', *Pacing and Clinical Electrophysiology*, 1999, 22, (10), pp. 1466-1475
- 45 Bacharova, L., Bang, L.E., Szathmary, V., and Mateasik, A.: 'Imaging QRS complex and ST segment in myocardial infarction', *Journal of Electrocardiology*, 2014, 47, (4), pp. 438-447
- 46 Sheridan, D.J., Culling, W., and Penny, W.J.: 'Electrophysiological Disturbances Associated with Acute Myocardial Infarction', *European Heart Journal*, 1986, 7, (suppl_B), pp. 11-18
- 47 Strauss, D.G., and Selvester, R.H.: 'The QRS complex—a biomarker that “images” the heart: QRS scores to quantify myocardial scar in the presence of normal and abnormal ventricular conduction', *Journal of Electrocardiology*, 2009, 42, (1), pp. 85-96
- 48 Surawicz, B., Childers, R., Deal, B.J., and Gettes, L.S.: 'AHA/ACCF/HRS Recommendations for the Standardization and Interpretation of the Electrocardiogram', *Circulation*, 2009, 119, (10), pp. e235-e240
- 49 Pudil, R., Feinberg, M.S., Hod, H., Boyko, V., Mandelzweig, L., and Behar, S.: 'The prognostic significance of intermediate QRS prolongation in acute myocardial infarction', *International Journal of Cardiology*, 2001, 78, (3), pp. 233-239

- 50 Adams, M.G., and Drew, B.J.: 'Body position effects on the ECG: Implication for ischemia monitoring', *Journal of Electrocardiology*, 1997, 30, (4), pp. 285-291
- 51 Tereshchenko, L.G., McNitt, S., Han, L., Berger, R.D., and Zareba, W.: 'ECG Marker of Adverse Electrical Remodeling Post-Myocardial Infarction Predicts Outcomes in MADIT II Study', *PLOS ONE*, 2012, 7, (12), pp. e51812
- 52 Somers, M.P., Brady, W.J., Perron, A.D., and Mattu, A.: 'The prominent T wave: Electrocardiographic differential diagnosis', *The American Journal of Emergency Medicine*, 2002, 20, (3), pp. 243-251
- 53 Montague, B.T., Ouellette, J.R., and Buller, G.K.: 'Retrospective review of the frequency of ECG changes in hyperkalemia', *Clin J Am Soc Nephrol*, 2008, 3, (2), pp. 324-330
- 54 Mandel, W.J., Burgess, M.J., Neville, J., Jr., and Abildskov, J.A.: 'Analysis of T-wave abnormalities associated with myocardial infarction using a theoretic model', *Circulation*, 1968, 38, (1), pp. 178-188
- 55 Hund, T.J., Decker, K.F., Kanter, E., Mohler, P.J., Boyden, P.A., Schuessler, R.B., Yamada, K.A., and Rudy, Y.: 'Role of activated CaMKII in abnormal calcium homeostasis and INa remodeling after myocardial infarction: Insights from mathematical modeling', *Journal of Molecular and Cellular Cardiology*, 2008, 45, (3), pp. 420-428
- 56 Decker, K.F., and Rudy, Y.: 'Ionic mechanisms of electrophysiological heterogeneity and conduction block in the infarct border zone', *Am J Physiol Heart Circ Physiol*, 2010, 299, (5), pp. H1588-1597
- 57 Moss, A.J., Zareba, W., Benhorin, J., Locati, E.H., Hall, W.J., Robinson, J.L., Schwartz, P.J., Towbin, J.A., Vincent, G.M., Lehmann, M.H., Keating, M.T., MacCluer, J.W., and Timothy, K.W.: 'ECG T-Wave Patterns in Genetically Distinct Forms of the Hereditary Long QT Syndrome', *Circulation*, 1995, 92, (10), pp. 2929-2934
- 58 Zenzemi, N., and Rodriguez, B.: 'Effects of L-type calcium channel and human ether-a-go-go related gene blockers on the electrical activity of the human heart: a simulation study', *EP Europace*, 2015, 17, (2), pp. 326-333
- 59 Borleffs, C.J.W., Scherptong, R.W.C., Man, S.-C., van Welsenes, G.H., Bax, J.J., van Erven, L., Swenne, C.A., and Schalij, M.J.: 'Predicting Ventricular Arrhythmias in Patients With Ischemic Heart Disease', *Circulation: Arrhythmia and Electrophysiology*, 2009, 2, (5), pp. 548-554
- 60 Engblom, H., Foster, J.E., Martin, T.N., Groenning, B., Pahlm, O., Dargie, H.J., Wagner, G.S., and Arheden, H.: 'The relationship between electrical axis by 12-lead electrocardiogram and anatomical axis of the heart by cardiac magnetic resonance in healthy subjects', *American Heart Journal*, 2005, 150, (3), pp. 507-512
- 61 Gnalini Sathanathan, S.Z., Gunjan Aggarwal, William Chik, Daniel Friedman, Aravinda Thiagalingam: 'Cardiac orientation: is there a correlation between the anatomical and the electrical axis of the heart?', *The British Journal of Cardiology*, 2015, 22, (2)
- 62 Peters, S.A.E., Bots, S.H., and Woodward, M.: 'Sex Differences in the Association Between Measures of General and Central Adiposity and the Risk of Myocardial Infarction: Results From the UK Biobank', *Journal of the American Heart Association*, 7, (5), pp. e008507
- 63 Fry, A., Littlejohns, T.J., Sudlow, C., Doherty, N., Adamska, L., Sprosen, T., Collins, R., and Allen, N.E.: 'Comparison of Sociodemographic and Health-Related Characteristics of UK Biobank Participants With Those of the General Population', *American Journal of Epidemiology*, 2017, 186, (9), pp. 1026-1034
- 64 Bhatnagar, P., Wickramasinghe, K., Williams, J., Rayner, M., and Townsend, N.: 'The epidemiology of cardiovascular disease in the UK 2014', *Heart*, 2015, 101, (15), pp. 1182
- 65 Littlejohns, T.J., Sudlow, C., Allen, N.E., and Collins, R.: 'UK Biobank: opportunities for cardiovascular research', *European Heart Journal*, 2019, 40, (14), pp. 1158-1166
- 66 Ronneberger, O., Fischer, P., and Brox, T.: 'U-Net: Convolutional Networks for Biomedical Image Segmentation', in Editor (Ed.)^(Eds.): 'Book U-Net: Convolutional Networks for Biomedical Image Segmentation' (Springer International Publishing, 2015, edn.), pp. 234-241

- 67 Li, S., Chen, Y., Yang, S., and Luo, W.: 'Cascade Dense-UNet for Prostate Segmentation in MR Images'. Proc. Intelligent Computing Theories and Application: 15th International Conference, ICIC 2019, Nanchang, China, August 3–6, 2019, Proceedings, Part I, Nanchang, China 2019 pp. Pages
- 68 Wang, T., Xu, X., Xiong, J., Jia, Q., Yuan, H., Huang, M., Zhuang, J., and Shi, Y.: 'ICA-UNet: ICA Inspired Statistical UNet for Real-Time 3D Cardiac Cine MRI Segmentation'. Proc. Medical Image Computing and Computer Assisted Intervention – MICCAI 2020: 23rd International Conference, Lima, Peru, October 4–8, 2020, Proceedings, Part VI, Lima, Peru 2020 pp. Pages
- 69 Kingma, D.P., and Ba, J.: 'Adam: A method for stochastic optimization', arXiv preprint arXiv:1412.6980, 2014
- 70 Robinette, K.M., Daanen, H., and Paquet, E.: 'The CAESAR project: a 3-D surface anthropometry survey', in Editor (Ed.)^(Eds.): 'Book The CAESAR project: a 3-D surface anthropometry survey' (1999, edn.), pp. 380-386
- 71 Pishchulin, L., Wuhrer, S., Helten, T., Theobalt, C., and Schiele, B.: 'Building statistical shape spaces for 3D human modeling', Pattern Recognition, 2017, 67, pp. 276-286
- 72 Rohr, K., Stiehl, H.S., Sprengel, R., Buzug, T.M., Weese, J., and Kuhn, M.H.: 'Landmark-based elastic registration using approximating thin-plate splines', IEEE Transactions on Medical Imaging, 2001, 20, (6), pp. 526-534
- 73 Villard, B., Grau, V., and Zacur, E.: 'Surface Mesh Reconstruction from Cardiac MRI Contours', in Editor (Ed.)^(Eds.): 'Book Surface Mesh Reconstruction from Cardiac MRI Contours' (2018, edn.), pp.
- 74 Engwirda, D.: 'Generalised primal-dual grids for unstructured co-volume schemes', Journal of Computational Physics, 2018, 375, pp. 155-176
- 75 Kaszynski, B.S.a.A.: 'PyVista: 3D plotting and mesh analysis through a streamlined interface for the Visualization Toolkit (VTK)', Journal of Open Source Software, 2019, 4, (37), pp. 1450
- 76 Banerjee, A., Camps, J., Zacur, E., Andrews, C.M., Rudy, Y., Choudhury, R.P., Rodriguez, B., and Grau, V.: 'A completely automated pipeline for 3D reconstruction of human heart from 2D cine magnetic resonance slices', Philosophical Transactions of the Royal Society A: Mathematical, Physical and Engineering Sciences, 2021, 379, (2212), pp. 20200257
- 77 <https://docs.pyvista.org/examples/01-filter/distance-between-surfaces.html#distance-between-two-surfaces>, accessed 31 January 2023

Figures and Tables

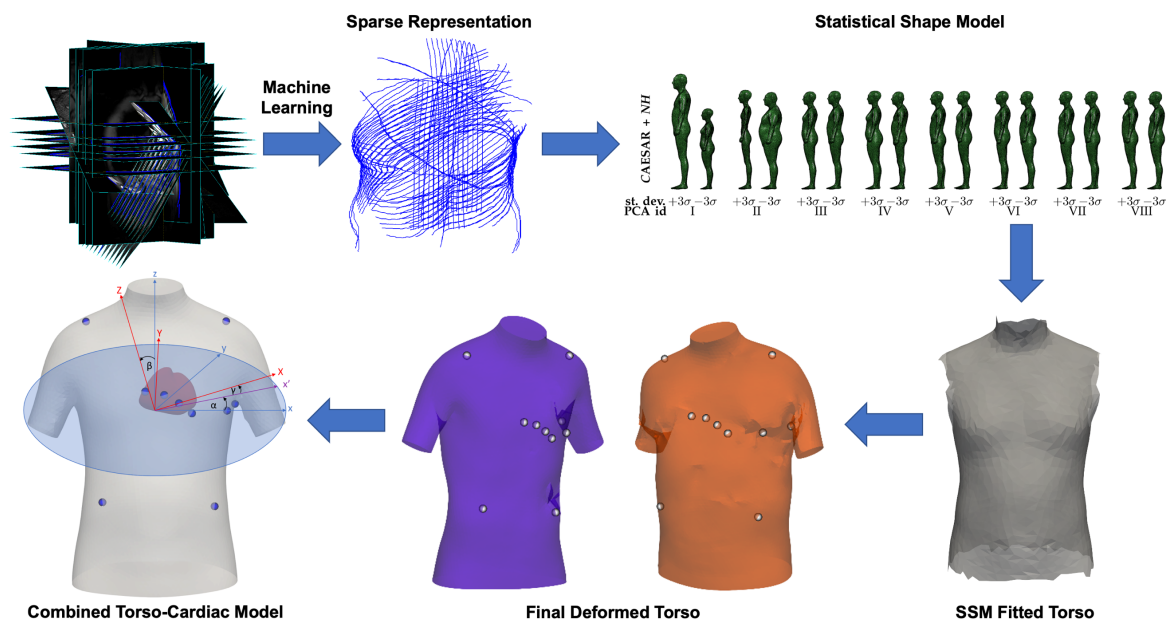
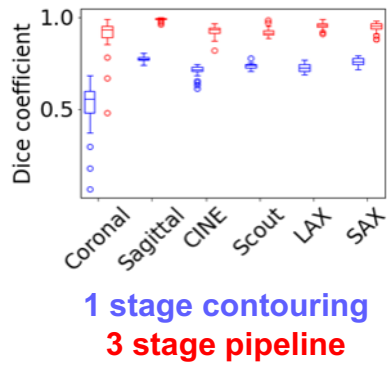
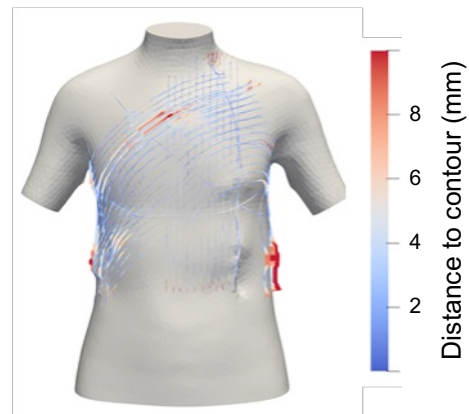


Figure 1. Proposed end-to-end automated 3D torso reconstruction pipeline from 2D standard clinical CMR scans. The image processing pipeline starts with selecting the localiser and scout CMR slices and applying a machine learning algorithm for automated torso contour extraction. A statistical shape model is applied over the sparse representation of the torso contours in 3D space to generate the initial fitted mesh, which is then deformed to generate the personalised 3D torso mesh. The combined torso-ventricular mesh is then utilised to extract the patient-specific geometry and biomarkers, including heart locations and orientations. Blue circles represent the positions of the ECG electrodes.

A. Contour extraction



B. Reconstruction quality



C. Error propagation

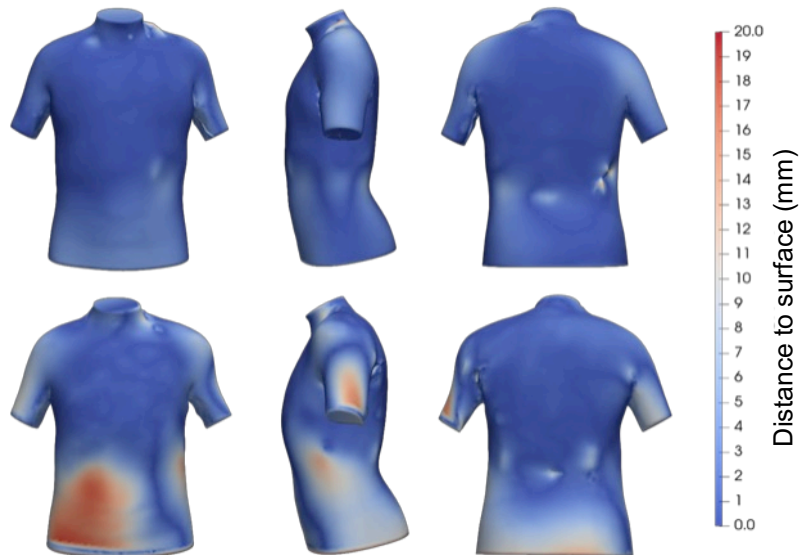


Figure 2. **A** comparison of Dice coefficient for different methods of contour extraction. Blue shows extraction using a single machine learning network directly from the input CMR images. Red demonstrates the improved accuracy using the three-stage segmentation, post-processing, and refinement pipeline. **B** surface-to-contour distance for an example case between the automatically reconstructed surface and the automatically generated torso contours. This demonstrates the quality of the reconstruction. **C** surface-to-surface distance between the torso mesh created using the automated pipeline and the manually annotated contours for the subjects with the smallest (upper panel) and largest (lower panel) electrode error respectively. This shows the error propagation from the contour determination to the surface generation.



Figure 3. **A, B** QRS duration across subjects for each ECG lead in healthy and post-MI subjects respectively with females shown as pale red circles and males as cyan triangles. **C** contribution of each parameter to the difference in QRS duration (QRSd) from females to males for healthy subjects, calculated by multiplying the regression coefficient for each factor by its mean difference between male and female populations. **D** correspondingly from females to males for post-MI subjects. **E, F** mean QRS durations across subjects for each ECG lead in males and females respectively. Healthy subjects are shown as black squares, post-MI subjects as red diamonds. **G** contribution of each parameter to the change in QRS duration from healthy to post-MI subjects in males, and **H** correspondingly from healthy to post-MI subjects in females, calculated by multiplying the regression coefficient for each factor by its mean difference between healthy and post-MI populations. Female y-axis limits have been adjusted by the difference in healthy QRS duration between sexes for ease of comparison.

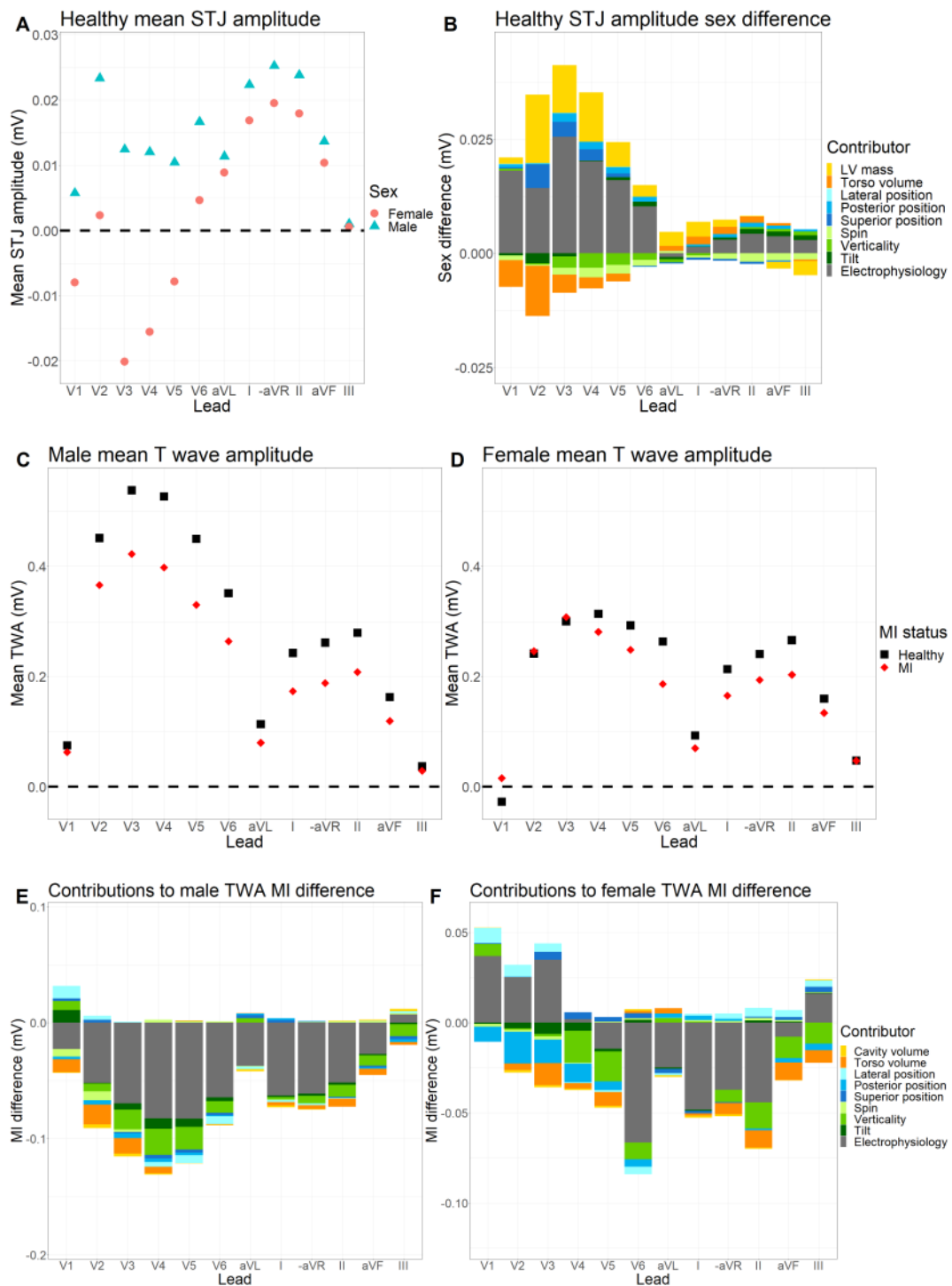


Figure 4. **A** mean ST amplitudes, measured at the J point, across subjects for each ECG lead in healthy subjects with females shown as pale red circles and males as cyan triangles. **B** contribution of each parameter to the difference in STJ amplitude from females to males for healthy subjects, calculated by multiplying the regression coefficient for each factor by its mean difference between male and female populations. Corresponding figures for post-MI subjects are shown in Supplemental Figure 5. **C, D** mean T wave amplitudes across subjects for each ECG lead in males and females respectively. Healthy subjects are shown as black squares, post-MI subjects as red diamonds. **E** contribution of each parameter to the change in T wave amplitude from healthy to post-MI subjects in males, and **F** correspondingly from healthy to post-MI subjects in females, calculated by multiplying the regression coefficient for each factor by its mean difference between healthy and post-MI populations. Female y-axis limits have been adjusted by the difference in healthy T wave amplitude between sexes for ease of comparison.

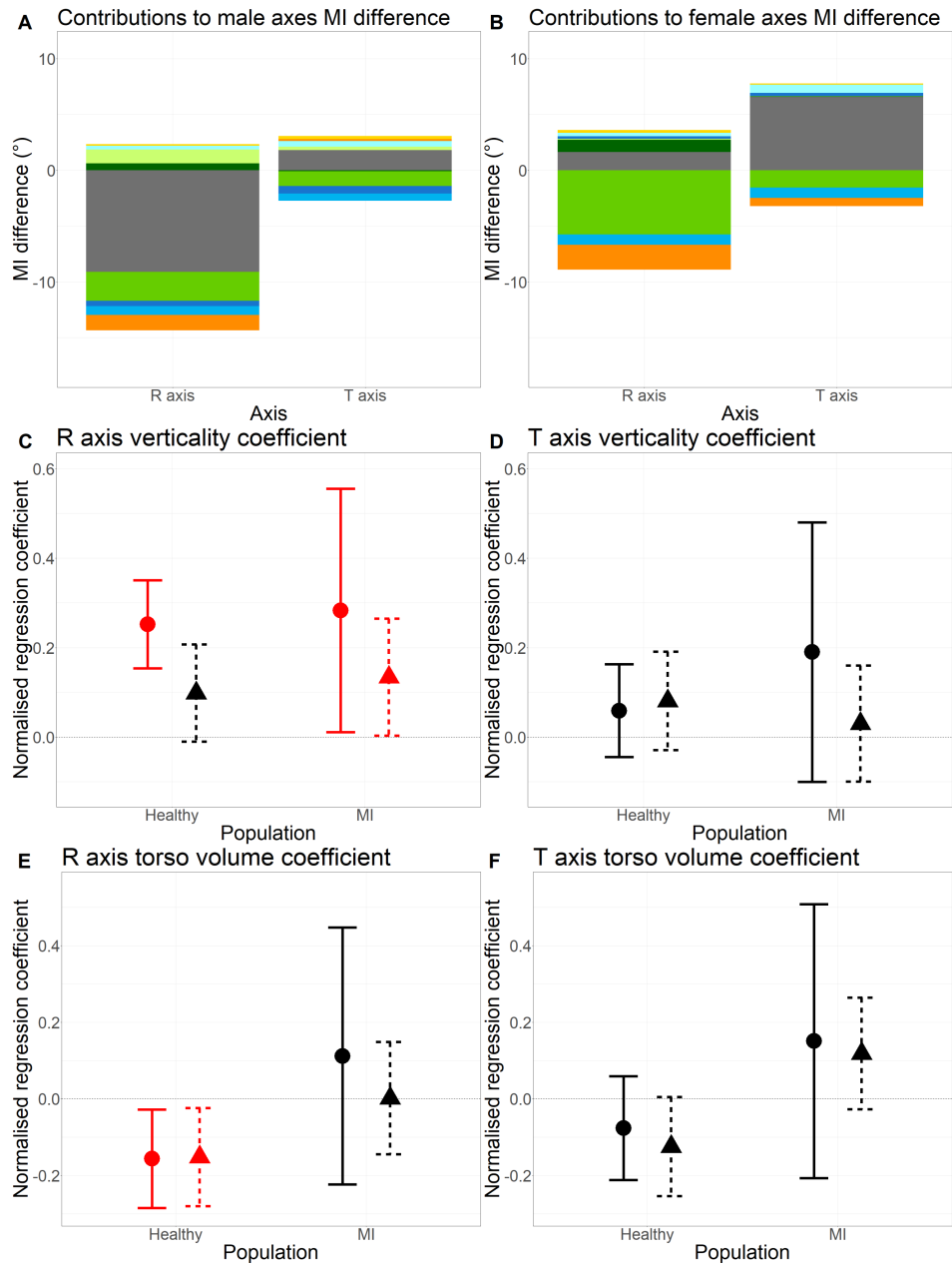


Figure 5. **A, B** contribution of each parameter to the change in axis angle from healthy to post-MI subjects in males and females respectively, calculated by multiplying the regression coefficient for each factor by its mean difference between healthy and post-MI populations. **C, D** normalised regression coefficients showing the association between the verticality of the cardiac long axis and the R and T axes respectively for the healthy and post-MI populations. Bars shown in red represent regression coefficients significantly different from 0, at a significance level of 0.05. **E, F** normalised regression coefficients showing the association between torso volume and the R and T axes respectively for the healthy and post-MI populations.

Table 1. Demographic characteristics of the 1476 subjects selected from the UK Biobank cohort.

Characteristics	Healthy (N = 1051)	MI (N = 425)	p-value
Age (years)	61.1 ± 7.5	67.3 ± 6.2	< 0.0001
Sex: Female, n (%)	581 (54.3)	84 (19.8)	< 0.0001
BMI (kg/m ²)	25.9 ± 4.1	28.1 ± 4.4	< 0.0001
Ethnicity, n (%)			0.5
White	1021 (97.1)	413 (97.2)	0.9742
Mixed	3 (0.3)	1 (0.2)	0.8667
Asian or Asian British	8 (0.8)	6 (1.4)	0.2430
Black or Black British	7 (0.7)	1 (0.2)	0.3075
Chinese	5 (0.5)	0 (0.0)	0.1543
Other ethnic group	5 (0.5)	2 (0.5)	0.9896
Prefer not to answer	2 (0.2)	2 (0.5)	0.3483

Continuous variables are shown as mean ± standard deviation and categorical variables as number of subjects (percentage in bracket). The p-value refers to the null hypothesis that the mean, or proportion in a category, is equal in the healthy and MI subpopulations. Distributions of continuous variables were tested for normality and equal variance, and the appropriate statistical test was selected, as outlined in the statistical methods. χ^2 -tests were performed to assess the proportions of subjects for categorical variables.